Tools for Computing the Capacitance of the Unit Cube and Laplace Eigenfunctions on the Sphere

Yong Su*

June 3, 2009

Abstract

Calculating the capacitance of a unit cube requires the numerical solution of a Laplace boundary value problem (BVP). However, current methods observe a slow algebraic error convergence. In this paper, we suggest the method of particular solutions (MPS) with domain decomposition technique to the BVP, which can handle the corner singularity of the cube and is spectrally accurate. The 2D analogous problem of calculating the capacity of the unit square with MPS is demonstrated, and for the 3D problem we focus on accurate methods to compute the needed basis functions based at the corner of the cube. This involves solving a Dirichlet boundary eigenvalue problem on 7/8 of a sphere. Fast algorithms for evaluating the required associated Legendre function are also discussed. We have obtained 15 digits accuracy in computing the capacity of the unit square with an exponential error convergence. For the related Dirichlet eigenvalue problem, we got 5 digits accuracy for the eigenvalues on the sphere.

1 Introduction

Computation of the electrical capacitance of a geometrically-complex conducting body is a common engineering problem, occurring for instance in

*Thesis paper under full supervision of Professor Alexander Barnett

designing micro-chip interconnects [13] or evaluating capacitances of biomembranes [10]. The self-capacitance of a unit cube in 3D space (i.e. $[-\frac{1}{2}, \frac{1}{2}]^3$ in $\mathbb{R}^3$) is a paradigm problem: as no analytical expression is known, a numerical approximation is crucial.

To numerically solve for the capacitance, we need to solve a boundary value problem (BVP), which is a partial differential equation (PDE) with conditions on surfaces for the function values. The BVP in question is Laplace's equation in a domain $\Omega \subset \mathbb{R}^n$, i.e. the PDE:

$$\Delta u = 0 \text{ in } \Omega \tag{1}$$

with the boundary condition:

$$u = f \text{ on } \partial\Omega \tag{2}$$

The capacitance is a linear functional of the solution u to the Laplace equation. Traditional methods to solve a PDE include finite difference method which represents the solution on a grid [18, p.1029], finite elements method (FEM) which represents the solution by polynomials on an irregular triangular mesh [20] and boundary integral equation (operator equation for unknown surface charge density) method [12].

However, owing to the corners and edges in a cube that will give rise to field singularities, standard numerical methods become difficult as we observe slow convergence to the true answer.

As a result, several numerical approaches have been developed to solve the above mentioned BVP and compute the value of the capacitance to high precision. One type of approach is deterministic such as using the boundary element method (BEM, also known as integral equation method) which is a finite-element approximation that uses quadrature to solve the boundary integral equation.

The idea is to segment the surface of a unit cube into N small pieces. Then, the problem can be turned into solving a set of linear equations that describe the dependence between segment potentials and charges [11]. Read [19] tries to extrapolate the number of subdivisions to infinity (Richardson extrapolation), though the best result he get has a relative error of magnitude 10^{-6}, along with an algebraic error convergence rate.

Another type of numerical approach depends on probabilistic random walk (Monte Carlo) simulations (since electrostatics is described by the same equation as steady-state diffusion). This type of method, so called "random

walk on the boundary" is claimed to be more efficient than the above deterministic methods and also holds the record of 7 digits as the highest accuracy currently known for the cube capacitance [14]. However, to reach 7-digit accuracy, 10^{14} trajectories are required because the Monte Carlo method only has an algebraic convergence rate of $1/\sqrt{N}$: this arises from standard result that the sample mean differs from true mean by $O(\sqrt{N})$ for sample size N.

To date, here is a table of most accurate digits obtained by previous researches:

Table 1: Previous Results for the Capacitance of the Unit Cube

Researcher	Method	Result
Read[19]	Refined BEM	$0.6606785 \pm 6 \times 10^{-7}$
Mascagni-Simonov[14]	Random Walk on $\partial\Omega$	$0.6606780 \pm 2.7 \times 10^{-7}$
Hwang-Mascagni[11]	Walk on Planes	$0.6606782 \pm 1 \times 10^{-7}$

Our project will develop a new spectrally accurate method that will produce an exponential error convergence with respect to N (the number of degree of freedom), which is faster than the algebraic convergence rate obtained by previous methods. With this method, we may finally be able to calculate the self-capacitance of a unit cube with much higher precision. In this work we will demonstrate the application of this method in the 2D case: i.e. calculating the capacity of a unit square and we will construct basis functions appropriate for the 3D cube capacitance problem (this in itself is a tricky task).

We notice that as the PDE (1) is a constant coefficient homogeneous PDE, we can therefore obtain the general solution to the boundary value problem by the method of particular solutions (MPS), summerized by the following steps [5]:

1. Find the particular solutions (basis functions) to the PDE above. For example, in polar coordinate system in $\mathbb{R}^2$, we can write basis ($n \in \mathbb{Z}$):

$$\xi_{2n}(r,\theta) = \begin{cases} r^n \cos n\theta, & n \neq 0 \\ 1, & n = 0 \end{cases} \tag{3}$$

and

$$\xi_{2n+1}(r,\theta) = \begin{cases} r^n \sin n\theta, & n \neq 0 \\ \log r, & n = 0 \end{cases} \tag{4}$$

2. Select a suitable basis (for instance, if $u(x) \sim 0$ when $x \to \infty$, then we have to restrict the above basis to $n < 0$). Next, we approximate the solution by the linear combination of possibly a subset of these basis functions: $u(x) = \sum_{i=1}^{N} c_i \xi_i(x)$, where $\{c_i\}$ is a set of coefficients.

3. Choosing boundary points p_j, $j = 1, 2, \cdots, m$ on $\partial\Omega$, we want the boundary conditions satisfied, i.e. $\sum_{i=1}^{N} c_i \xi_i(y_j) = f(y_j)$ for $1 \leq j \leq m$. This turns out to be solving a linear system $A\mathbf{c} = \mathbf{b}$, and we choose the least-square solution that gives the minimum l_2 error in the boundary point vector, hence a good approximation to the minimum boundary error in $L^2(\partial\Omega)$ norm.

In order to adopt the method of particular solutions with basis functions adapted to the cubical corners, we need to use domain-decompositon techniques [3]: although the corner lives in one domain, expansion of the solution at ∞ lies in a different domain. Generally speaking, we can divide Ω into two parts: $\Omega = \Omega_1 + \Omega_2$, and we denote $\Gamma = \overline{\Omega_1} \cap \overline{\Omega_2}$ as the intersection of the two sub-domains. Then, according to the method of particular solutions, we can find solution u_1 in Ω_1 and u_2 in Ω_2. Finally, to get the solution on the whole domain Ω, we only need to match the sub-domain solutions on Γ, i.e. $u_1 = u_2$ and also match their normal derivatives on Γ: define n as the normal vector on Γ into Ω_1 but out of Ω_2, then $\partial_n u_1 = \partial_n u_2$. The new matching errors (i.e. the L^2 norms) have to be incorporated into the least square error we mentioned before: we will now minimize $\|u_1 - u_2\|_{L^2(\Gamma)} + \|\partial_n u_1 - \partial_n u_2\|_{L^2(\Gamma)} + \|u - f\|_{L^2(\partial\Omega)}$.

However, because of the separation of variables, computing these basis functions involves a Dirichlet eigenvalue problem on the sphere with one octant removed, which is a difficult problem in itself due to the singular corners of the octant. In this project we first present the analogous problem in 2D and solve the capacity for unit square in Section 2. Next, we introduce the 3D capacitance problem in Section 3, which translates to solving an eigenvalue problem on part of the sphere in Sections 4-5. We then focus on accurate methods to solve this eigenvalue problem, using again the MPS through Sections 7-9. We will also discuss fast methods for evaluating the needed associated Legendre functions via recurrence relations in Section 6.

2 Application of MPS with Domain Decomposition to unit square in 2D

Let $S \subset \mathbb{R}^2$ be a bounded closed domain that is compact on $\mathbb{R}^2$ and $\Omega = \mathbb{R}^2 \setminus S$. If u is a unique solution that satisfies the following Laplace equation with Dirichlet boundary data on $\partial\Omega$ (Fig. 1):

$$\begin{aligned} \Delta u &= 0 \text{ in } \Omega & (5)\\ u &= 0 \text{ on } \partial\Omega & (6)\\ u(x) &\sim \log|x| + O(1) \text{ as } |x| \to \infty & (7) \end{aligned}$$

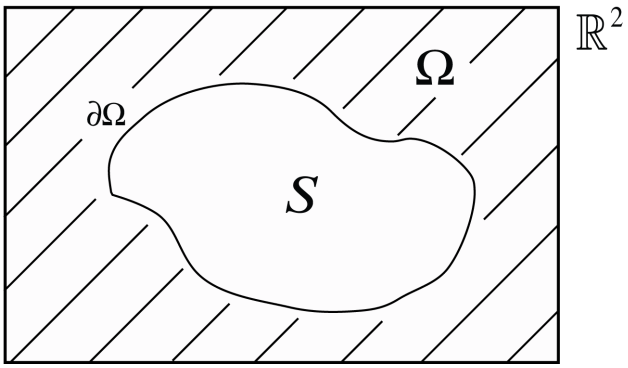

Figure 1: 2D general domain for the Laplace Equation

Here, the sign '$\sim$' means 'is asymptotic to'. In our example, this means there exists constants $M > 0$ and $K > 0$, such that $|u(x) - \log|x|| < M$ for all $|x| > K$.

Then, the following limit exisits and is called a Robin constant of S [6]:

$$\lim_{|x|\to\infty} (u(x) - \log|x|) =: \alpha \tag{8}$$

We thus define the (logarithmic) capacity of S on the plane $\mathbb{R}^2$ to be

$$c(S) = e^{-\alpha}. \tag{9}$$

Consider the special case when $S = [-\frac{1}{2}, \frac{1}{2}]^2$ (i.e. S is a unit square centered at the origin). (Fig. 2) The exact value of its capacity is known analytically: $c(S) = \frac{1}{4\pi^{3/2}} \cdot \Gamma(\frac{1}{4})^2$ [8]. We want to test if we can use MPS

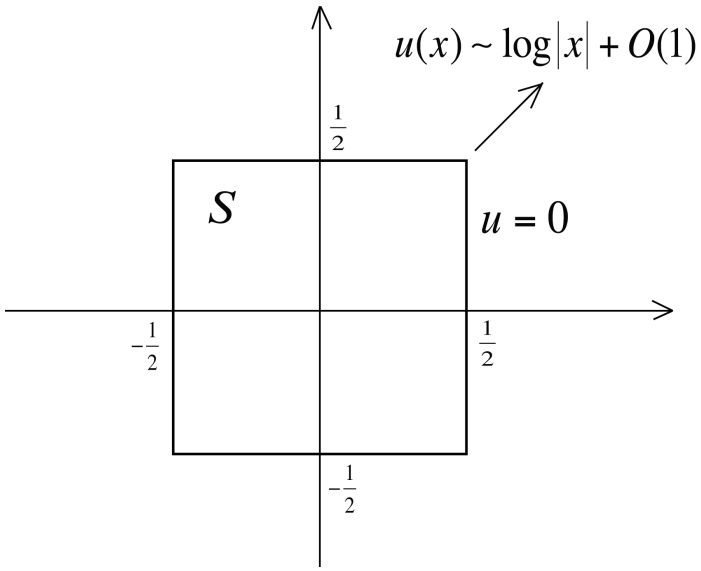

Figure 2: 2D Laplace Equation with unit square domain

with domain-decomposition techniques to get a high-precision numerical approximation of u. If successful, these methods would be worth pursuing in 3D.

If we naively use the basis functions ξ_{2n} or ξ_{2n+1} outside the square (this requires $n \leq 0$, as we will see later), we will get into trouble with convergence when we approach the corner of the square because the corner is singular [5](i.e. the exterior angle of the corner is of the form π/n for some $n \in \mathbb{N}$. We also notice that the normal on the corner is ill-defined in our case). Instead we place an artificial circle outside the square (for example, a circle centered at the origin with $R = 1.5$) and separately solve the Laplace equation inside and outside the circle using MPS so we can match up on the boundaries. Due to the geometric symmetry of the square and the circle, we only need to look at the red-shaded region illustrated in Fig. 3.

First, let us consider the solution in region A, which is outside the circle. If we write

$$v(r, \theta) = u(r, \theta) - \log r, \tag{10}$$

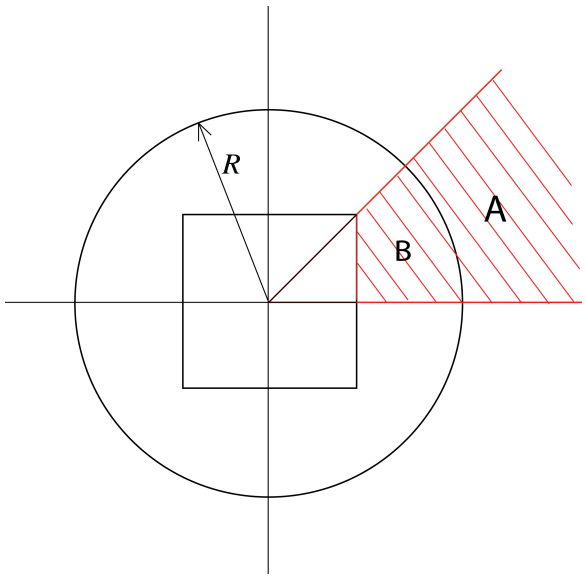

Figure 3: The artificial circle boundary used to match solution in region A to region B. The unit square is also shown.

then v must satisfy the following Laplace equation:

$$\begin{aligned} \Delta v &= 0 \text{ in } \Omega && (11)\\ v &= -\log r \text{ on } \partial\Omega && (12)\\ v &\sim O(1) \text{ as } r \to +\infty && (13) \end{aligned}$$

Since v is harmonic at infinity, we use basic functions in the form $r^{-n}\sin n\theta$ for $n \geq 1$ or $r^{-n}\cos n\theta$ for $n \geq 0$. (Note we have used the fact that outside the disk, a Laurent expansion is complete.)

Also, since the solution u preserves the symmetry of the square and the boundary conditions, we need these basis functions to be even symmetric on the lines $\theta = 0$ and $\theta = \pi/4$.

Thus the only basis functions we can use are of the form $\xi_n(r,\theta) = r^{-4n}\cos(4n\theta)$, $n = 0, 1, 2, \cdots$.

In other words,

$$v(r,\theta) = \sum_{i=0}^{N} c_i \xi_n(r,\theta) \qquad (14)$$

where $\{c_i\}$ are undetermined coefficients.

Note that here it is important that we start with the index $i = 0$ instead of with the index $i = 1$. This is because at exterior, the function v really is $O(1)$ plus a harmonic function that dies at infinity. As a result, a constant term should be included in the set of basis functions.

Now we consider the solution in the region B. To simplify the expression of u, we switch the polar coordinate system (centered at O) to be centered at M, the top-right corner of the square, which can be illustrated in Fig. 4.

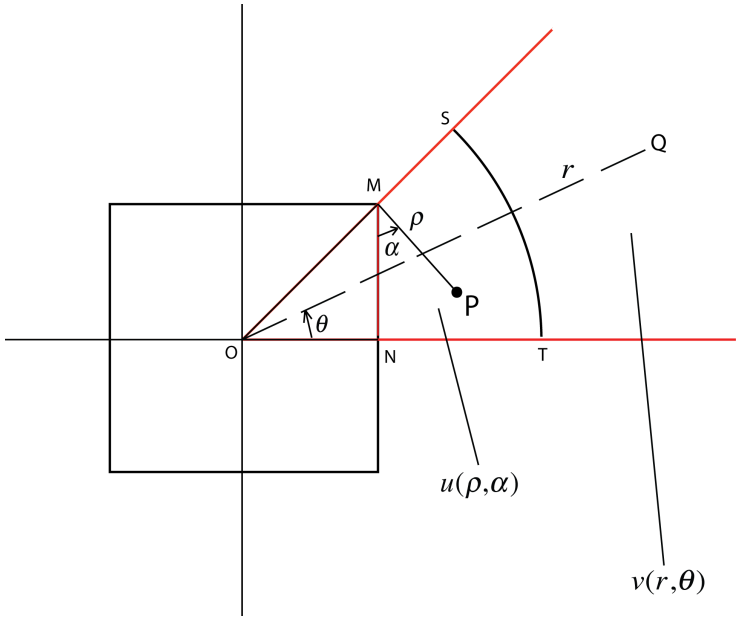

Figure 4: Solution $u(\rho, \alpha)$ in region B, with polar coordinate system centered at M. Solution $v(r, \theta)$ in region A with polar coordinate system centered at O is also shown.

We now use separation of variables appropriate for the corner region. Since the solution u has to satisfy the boundary data on segment MN (i.e. $u(\rho, 0) = 0$) and it has to preserve symmetry according to the line $\alpha = 3\pi/4$, we can only use basis functions of the form:

$$\varphi_n(\rho, \alpha) = \rho^{2(2n-1)/3} \cdot \sin(\frac{2(2n-1)\alpha}{3}),\ n \in \mathbb{N} \tag{15}$$

Hence, we can write u as a linear combination of these basis functions:

$$u(\rho, \alpha) = \sum_{i=1}^{N} a_i \varphi_i(\rho, \alpha), \tag{16}$$

where $\{a_i\}$ are also undetermined coefficients. It is this corner expansion that allows us high (spectral) accuracy.

We denote $\mathbf{b} = (a_1, a_2, \cdots, a_N, c_0, c_1, c_2, \cdots, c_N)^T$ the coefficient vector. To solve for $\mathbf{b}$, we need to match up all the boundary conditions. In fact, there are three boundary conditions we need to fit (1) function values on the arc $\widehat{ST}$, (2) normal derivatives on the line segment NT and (3) normal derivatives on $\widehat{ST}$:

(1) Let R denote the radius of our imaginary circle. If we choose a Gaussian quadrature $\theta_1, \theta_2, \cdots, \theta_m$ on $[0, \pi/4]$, we can place m corresponding nodes $n_1, n_2, \cdots, n_m$ on $\widehat{ST}$, where $n_i = (R, \theta_i)$ in polar coordinate system. Now, u and v has to agree on these m nodes, with a jump $\log R$ because of (10). (Fig. 5)

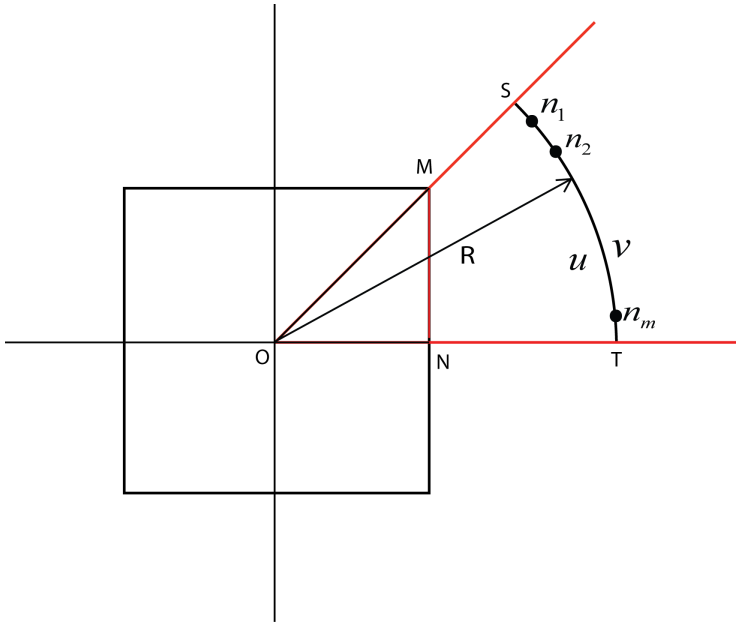

Figure 5: Matching u and v with nodes $n_1, n_2, \cdots, n_m$ on the boundary $\widehat{ST}$

In other words, the following m linear equations must hold:

$$\sum_{i=1}^{N} a_i\varphi_i(n_1) \quad - \quad \sum_{j=1}^{N} c_j\xi_{j-1}(n_1) = \log R \tag{17}$$

$$\sum_{i=1}^{N} a_i\varphi_i(n_2) \quad - \quad \sum_{j=1}^{N} c_j\xi_{j-1}(n_2) = \log R \tag{18}$$

$$\cdots \tag{19}$$

$$\sum_{i=1}^{N} a_i\varphi_i(n_m) \quad - \quad \sum_{j=1}^{N} c_j\xi_{j-1}(n_m) = \log R \tag{20}$$

We have to be cautious since $\varphi_k(n_j)$ and $\xi_k(n_j)$ are actually using different coordinate systems as we have discussed before.

For future convenience, we denote:

$$S_1 = \begin{bmatrix} \varphi_1(n_1) & \varphi_2(n_1) & ... & \varphi_N(n_1) & -\xi_0(n_1) & -\xi_1(n_1) & ... & -\xi_{N-1}(n_1) \\ \varphi_1(n_2) & \varphi_2(n_2) & ... & \varphi_N(n_2) & -\xi_0(n_2) & -\xi_1(n_2) & ... & -\xi_{N-1}(n_2) \\ ... & ... & ... & ... & ... & ... & ... & ... \\ \varphi_1(n_m) & \varphi_2(n_m) & ... & \varphi_N(n_m) & -\xi_0(n_m) & -\xi_1(n_m) & ... & -\xi_{N-1}(n_m) \end{bmatrix}$$

(2) If we place m Guassian nodes $t_1, t_2, \cdots, t_m$ on the line segment NT, then the normal derivative of u on each of the node t_j should always equal zero because we want u to have correct symmetry. (Fig. 6)

Notice that in polar coordinate system (ρ, r), $\overrightarrow{\nabla} = (\frac{\partial}{\partial\rho}, \frac{1}{\rho}\frac{\partial}{\partial\alpha})$. Hence, the normal derivative of a basis function φ_k on node t_j can be calculated as:

$$\frac{\partial}{\partial n}\varphi_k(\rho_j, \alpha_j) = -\cos\alpha \cdot \frac{\partial\varphi_k}{\partial\rho}(\rho_j, \alpha_j) + \sin\alpha \cdot \frac{1}{\rho} \cdot \frac{\partial\varphi_k}{\partial\alpha}(\rho_j, \alpha_j) \tag{21}$$

We therefore require the following linear equations to hold:

$$\sum_{j=1}^{N} a_j\varphi_{\hat{n}_j}(t_1) = 0 \tag{22}$$

$$\sum_{j=1}^{N} a_j\varphi_{\hat{n}_j}(t_2) = 0 \tag{23}$$

$$\cdots \tag{24}$$

$$\sum_{j=1}^{N} a_j\varphi_{\hat{n}_j}(t_m) = 0 \tag{25}$$

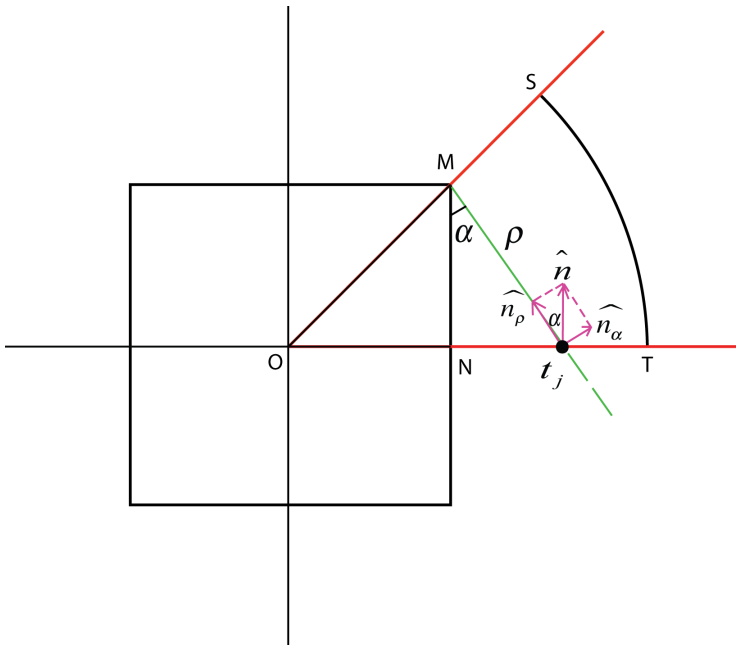

Figure 6: Normal derivative of u at node t_j on NT

Let us write:

$$S_2 = \begin{bmatrix} \varphi_{\hat{n}_1}(t_1) & \varphi_{\hat{n}_2}(t_1) & \dots & \varphi_{\hat{n}_N}(t_1) & 0 & 0 & \dots & 0 \\ \varphi_{\hat{n}_1}(t_2) & \varphi_{\hat{n}_2}(t_2) & \dots & \varphi_{\hat{n}_N}(t_2) & 0 & 0 & \dots & 0 \\ \dots & \dots & \dots & \dots & \dots & \dots & \dots & \dots \\ \varphi_{\hat{n}_1}(t_m) & \varphi_{\hat{n}_2}(t_m) & \dots & \varphi_{\hat{n}_N}(t_m) & 0 & 0 & \dots & 0 \end{bmatrix}$$

(3) Finally, the normal derivative of u and v must agree on the node n_j, $j = 1, 2, \cdots, m$ (Fig. 7):

Same as what we have done in (2), the normal derivative of a basis function φ_k on node n_j can be calculated as:

$$\frac{\partial}{\partial n}\varphi_k(\rho_j, \alpha_j) = n_\rho \cdot \frac{\partial \varphi_k}{\partial \rho}(\rho_j, \alpha_j) + n_\alpha \cdot \frac{\partial \varphi_k}{\partial \alpha}(\rho_j, \alpha_j), \tag{26}$$

where $n_\rho = \cos\beta$, $n_\alpha = \sin\beta$ and $\beta = \pi/2 + \theta - \alpha$.

On the other hand, since the unit normal derivative $\hat{n}$ at node n_j agrees with the direction of $\hat{r}$ at node n_j in the polar system (r, θ), we have:

$$\frac{\partial}{\partial n}\xi_k(r_j, \theta_j) = 1 \cdot \frac{\partial \xi_k}{\partial r}(r_j, \theta_j) + 0 \cdot \frac{1}{r}\frac{\partial \xi_k}{\partial \theta}(r_j, \theta_j) = \frac{\partial \xi_k}{\partial r}(r_j, \theta_j) \tag{27}$$

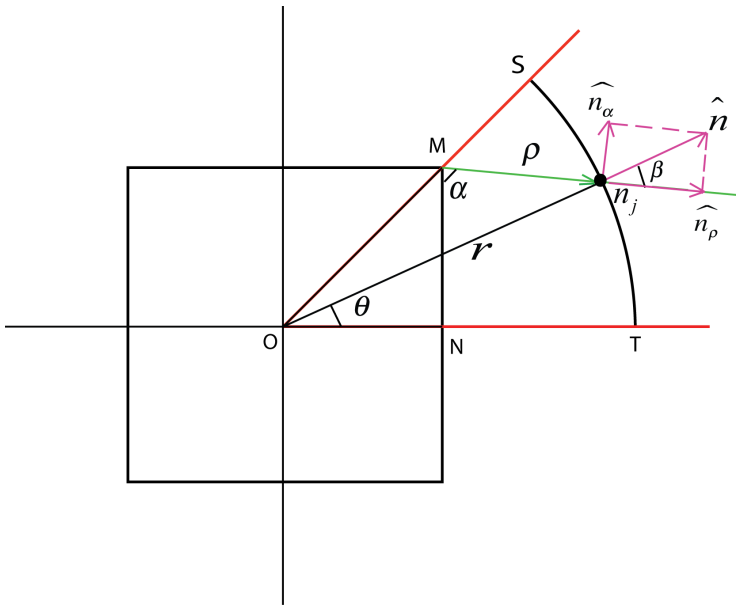

Figure 7: Matching the normal derivative of u and v on $\widehat{ST}$

Adding the jump in the values of $\frac{\partial}{\partial n}v$ compared to $\frac{\partial}{\partial n}u$, the following linear equations mush hold:

$$\sum_{i=1}^{N} a_i \varphi_{n_i}(n_1) \quad - \quad \sum_{j=1}^{N} c_j \xi_{n_{j-1}}(n_1) = 1/R \tag{28}$$

$$\sum_{i=1}^{N} a_i \varphi_{n_i}(n_2) \quad - \quad \sum_{j=1}^{N} c_j \xi_{n_{j-1}}(n_2) = 1/R \tag{29}$$

$$\cdots \tag{30}$$

$$\sum_{i=1}^{N} a_i \varphi_{n_i}(n_1) \quad - \quad \sum_{j=1}^{N} c_j \xi_{n_{j-1}}(n_1) = 1/R \tag{31}$$

Again, write:

$$S_3 = \begin{bmatrix} \varphi_{\hat{n}_1}(n_1) & \varphi_{\hat{n}_2}(n_1) & \ldots & \varphi_{\hat{n}_N}(n_1) & -\xi_{\hat{n}_0}(n_1) & -\xi_{\hat{n}_1}(n_1) & \ldots & -\xi_{\hat{n}_{N-1}}(n_1) \\ \varphi_{\hat{n}_1}(n_2) & \varphi_{\hat{n}_2}(n_2) & \ldots & \varphi_{\hat{n}_N}(n_2) & -\xi_{\hat{n}_0}(n_2) & -\xi_{\hat{n}_1}(n_2) & \ldots & -\xi_{\hat{n}_{N-1}}(n_2) \\ \ldots & \ldots & \ldots & \ldots & \ldots & \ldots & \ldots & \ldots \\ \varphi_{\hat{n}_1}(n_m) & \varphi_{\hat{n}_2}(n_m) & \ldots & \varphi_{\hat{n}_N}(n_m) & -\xi_{\hat{n}_0}(n_m) & -\xi_{\hat{n}_1}(n_m) & \ldots & -\xi_{\hat{n}_{N-1}}(n_m) \end{bmatrix}$$

Now we have listed all the linear conditions that have to be imposed on

u and v, it's time to solve for the whole linear system:

Let $A = \begin{bmatrix} S_1 \\ S_2 \\ S_3 \end{bmatrix}$, $\mathbf{c} = (\log R, \log R, \cdots, \log R, 0, 0, \cdots, 0, \frac{1}{R}, \frac{1}{R}, \cdots, \frac{1}{R})^T$.

Thus the linear system is just $A\mathbf{b} = \mathbf{c}$ and we can solve for the coefficient vector $\mathbf{b}$ using Matlab's least-squares dense solver.

If we let $N = 20$ and $m = 60$, here is the final solution of u in contour plot (Fig. 8):

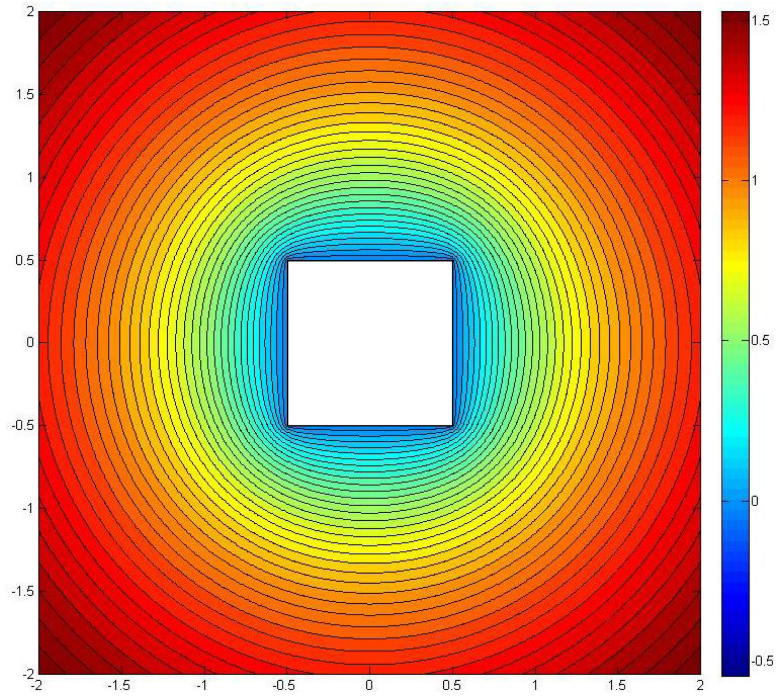

Figure 8: Contour plot for the solution u with $N = 20$ and $m = 60$

These graphs clearly indicate that the boundary data is well satisfied and contours tend to circles as $|x| \to \infty$.

In fact, if we plot the norm $||A\mathbf{b} - \mathbf{c}||$ (which indicates roughly within a small constant L^2 norm of the matching error on the boundary), we will get an exponential convergence as shown in Fig. 9.

Finally, the c_0 term in the solved vector $\mathbf{b}$ is an approximation to the constant Robin coefficient α. We know that the true capacity is 0.590170299508 up to machine precision. According to the second definition of the capacity

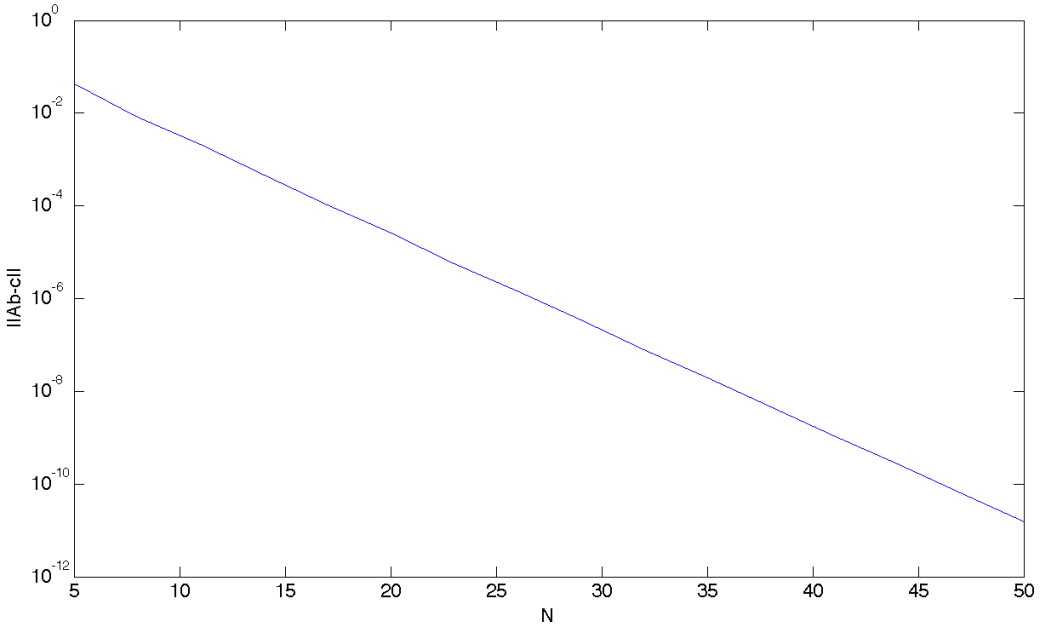

Figure 9: Least square error $||A\mathbf{b} - \mathbf{c}||$ against N showing exponential convergence

$C = e^{-\alpha}$, we test how fast our solution converges to the true value in Fig. 10. As expected, we get an exponential error convergence: i.e. we need roughly 3-4 basis functions per decimal digit achieved.

3 3D Laplace Equation

Mathematically, the capacitance of a unit cube $S = [-\frac{1}{2}, \frac{1}{2}]^3$ can be expressed as the surface flux of solution field f satisfying the following Laplace Equation in $\mathbb{R}^3$ with Dirichlet boundary data ($\Omega =: \mathbb{R}^3 \setminus S$):

$$\Delta f = 0 \text{ in } \Omega \tag{32}$$

$$f = 0 \text{ on } \partial\Omega \tag{33}$$

$$f(x) \sim 1 + o(1) \text{ as } |x| \to \infty \tag{34}$$

Assume n is the normal pointing away from S, into Ω. The capacitance

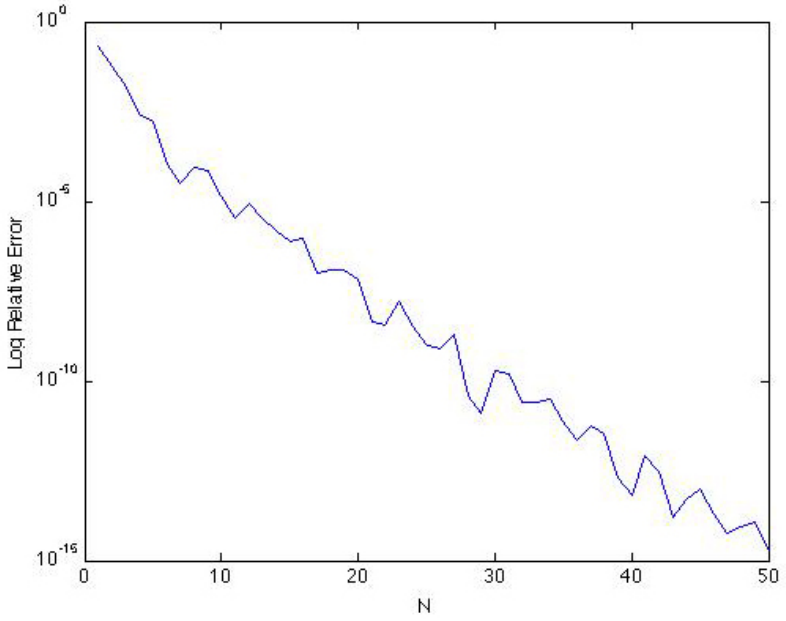

Figure 10: log relative error of the capacity against N, showing exponential convergence

of the unit cube is defined as

$$c(S) = \int_{\partial\Omega} \frac{\partial f}{\partial n} ds. \tag{35}$$

It is well known that the solution f satisfies the following asymptotic condition [7, p.164]:

$$f(x) \sim 1 + \frac{a}{r} + o(\frac{1}{r}). \tag{36}$$

Imagine a sphere $E := \{x : |x| < R_e, x \in \Omega\}$ outside the cube. Using the fact that f is a harmonic function and apply the Divergence Theorem to ∇f, we know that the surface integral of $\partial f/\partial n$ vanishes on any closed boundary. Choose the boundary $E \setminus S$, we have:

$$c(S) = \int_{\partial\Omega} \frac{\partial f}{\partial n} ds = \int_{\partial E} \frac{\partial f}{\partial n} ds = 4\pi a, \tag{37}$$

where a is the monopole coefficient in (36).

To solve for f, we imagine a sphere with radius R centered at corner O of the cube (Fig. 11). This is needed, as it is needed in the 2D case, to explicitly write a set of basis functions adapted for the singularity of f at the corner.

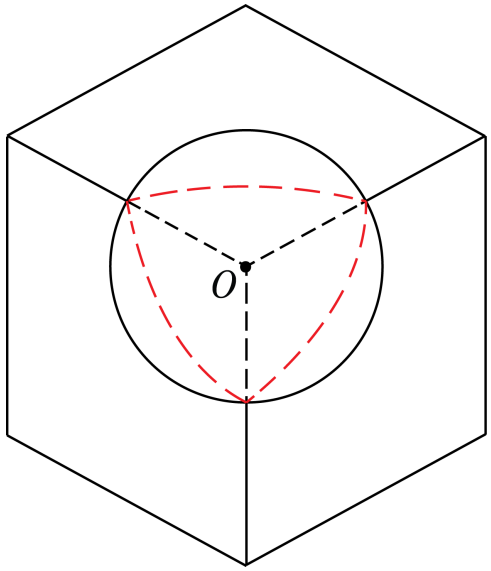

Figure 11: Sphere centered at the corner of the cube

We define a conical domain to be the surface of a cone-shaped region with base $D \in \mathbb{S}^2$, as shown in Fig. 12. We see that when Ω is the exterior of the unit cube, it is locally identical (i.e. identical up to a certain radius) to a conical domain about any corner.

Now, consider the spherical coordinate system (r, θ, φ) centered at corner O (θ can be understood as the elevation, or the latitude, while φ is the azimuthal, or the longitude). Denote $S^2 = \{(R, \theta, \varphi) : 0 \leq \theta \leq \pi, 0 \leq \varphi < 2\pi\}$ the surface of the sphere. Let D be the sphere surface with $1/8$ removed: $D = S^2 \setminus \{(R, \theta, \varphi) : -\pi/2 < \varphi < 0 \text{ and } 0 < \theta < \pi/2\} = \{(R, \theta, \varphi) : 0 < \varphi < 3\pi/2 \text{ or } \theta > \pi/2\}$. Then, the corner domain we are interested in is a conical domain with base D (Fig. 13).

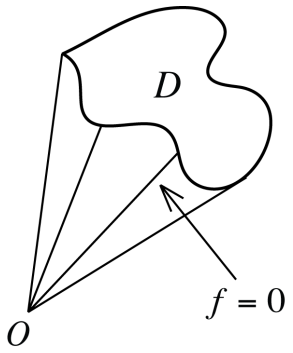

Figure 12: A conical domain with D on the sphere S^2

4 The Eigenvalue Problem on the 7/8 Sphere

Next, we convert the three-dimensional Laplace Equation into the spherical coordinate system (r, θ, φ) (centered at corner O) [7]:

$$\Delta f = \frac{1}{r^2} \cdot \frac{\partial}{\partial r}(r^2 \cdot \frac{\partial f}{\partial r}) + \frac{1}{r^2 \sin\theta} \cdot \frac{\partial}{\partial \theta}(\sin\theta \cdot \frac{\partial f}{\partial \theta}) + \frac{1}{r^2 \sin^2\theta} \cdot \frac{\partial^2 f}{\partial \varphi^2} = 0 \quad (38)$$

Note that the latter two terms in the right hand side of the above equation (38) have no r component besides the common term $1/r^2$, so we can combine these two terms and rewrite the equation as

$$\Delta f = \Delta_r f + \frac{1}{r^2}\Delta_{S^2} f = 0, \quad (39)$$

where Δ_{S^2} stands for the Laplacian on the sphere S^2: i.e. $\Delta_{S^2} f(\theta, \varphi) = \frac{1}{\sin\theta}\partial_\theta(\sin\theta \partial_\theta f) + \frac{1}{\sin^2\theta}\frac{\partial^2 f}{\partial \varphi^2}$.

Since the boundary condition $f = 0$ does not change with respect to the radial component in the conical domain (Fig. 12), we can separate the radial part in f and assume

$$f(r, \theta, \varphi) = R(r)T(\theta, \varphi). \quad (40)$$

Let us show that the radial part $R(r) = r^\nu$ is the correct separable solution. Since $\Delta f = Tr^2\Delta_r R + R\Delta_{S^2} T = 0$, we have:

$$\frac{r^2\Delta_r R}{R} + \frac{\Delta_{S^2} T}{T} = 0. \quad (41)$$

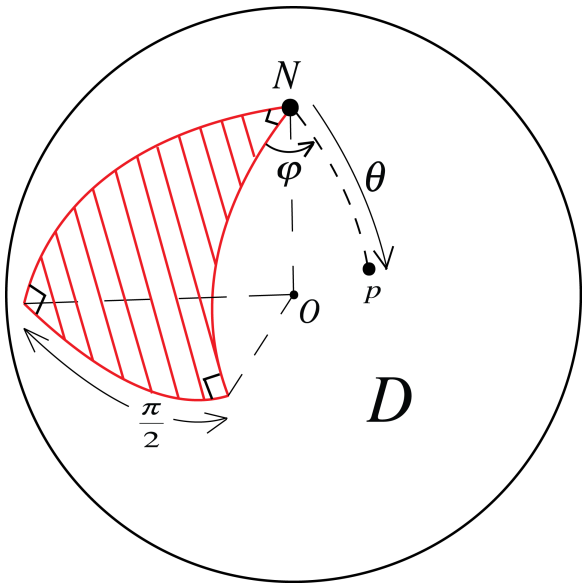

Figure 13: 7/8 of the sphere, showing coordinate system (θ, φ)

Hence $\frac{r^2\Delta_r R}{R}$ is a constant, let it be $\nu(\nu+1)$. We have $(r^2R')' = \nu(\nu+1)R$, or

$$r^2R'' + 2rR' - \nu(\nu+1)R = 0. \tag{42}$$

(42) is a second-order homogeneous Cauchy-Euler equation, it's easy to find that $R = r^\nu$ is the solution we need.

Now, plugging in $R = r^\nu$, equation (39) becomes

$$\Delta f = T\Delta_r r^\nu + r^\nu \frac{1}{r^2}\Delta_{s^2} T = 0. \tag{43}$$

Simplifying the equation (43), we obtain

$$-\Delta_{S^2} T = \nu(\nu+1)T. \tag{44}$$

As a result, we have to deal with a Dirichlet eigenvalue problem (EVP) for T on $D \subset S^2$, 7/8 of the sphere:

$$-\Delta_{S^2} T = \nu(\nu+1)T \text{ in } D \tag{45}$$

$$T = 0 \text{ on } \partial D \tag{46}$$

The eigenvalues $\nu_1, \nu_2, \cdots$ will give us the power in the radial part of the basis functions, while the corresponding $T_1, T_2, \cdots$ will give us the eigenfunctions.

5 Helmholtz Basis Functions on S^2: Associated Legendre Functions

Rearrange the equation (44), we have a Helmholtz equation on S^2:

$$(\Delta_{S^2} + \nu(\nu+1))T = 0. \tag{47}$$

We will approximate T by a sum of basis functions $\sum c_i \xi_i(\theta, \varphi)$, where each $\xi \in \{\xi_i\}$ is a separable basis function which can be computed analytically.

Aassume that $\xi(\theta, \varphi) = P(\theta)Q(\varphi)$. Plugging into the equation (47), we obtain:

$$PQ \cdot \nu(\nu+1) + \frac{Q}{\sin\theta} \cdot \frac{d}{d\theta}(\sin\theta \cdot \frac{dP}{d\theta}) + \frac{P}{\sin^2\theta} \cdot \frac{d^2Q}{d\varphi^2} = 0. \tag{48}$$

In order to apply MPS to get an approximation of T, we need to find basis functions on S^2 which are particular solutions to the equation (47). Rearrange the equation (48), we get:

$$\sin^2\theta \cdot \{\nu(\nu+1) + \frac{1}{P\sin\theta} \cdot \frac{d}{d\theta}(\sin\theta \cdot \frac{dP}{d\theta})\} + \frac{1}{Q} \cdot \frac{d^2Q}{d\varphi^2} = 0 \tag{49}$$

Thus $\frac{1}{Q} \cdot \frac{d^2Q}{d\varphi^2}$ is a constant: $\frac{1}{Q} \cdot \frac{d^2Q}{d\varphi^2} = -\mu^2$. This gives us the solution $Q = e^{\pm i\mu\varphi}$ for the azimuthal function. Note that the dependence of Q will be chosen to explicitly handle corner singularity at N.

On the other hand, we can also rearrange the equation (48) to separate P:

$$\frac{1}{\sin\theta} \cdot \frac{d}{d\theta}(\sin\theta \cdot \frac{dP}{d\theta}) + \{\nu(\nu+1) - \frac{\mu^2}{\sin^2\theta}\} \cdot P = 0. \tag{50}$$

Let $x = \cos\theta$, the above equation (50) can be rewritten as

$$(1-x^2) \cdot \frac{d^2P}{dx^2} - 2x \cdot \frac{dP}{dx} + \{\nu(\nu+1) - \frac{\mu^2}{1-x^2}\} \cdot P = 0. \tag{51}$$

The solution to the equation (51) when $|x| < 1$ is called the associated Legendre function (on the cut), where the parameters μ and ν are called order and degree alternatively [17]. We denote the solution P with parameters ν, μ as $P_\nu^{\pm\mu}(x)$.

As Olver explains in his paper [17], solutions which remain bounded as $\theta \to 0$ are denoted $P_\nu^{-\mu}(x)$ with $\mu > 0$. So from now on, we will only refer the solution P in the form $P_\nu^{-\mu}(x)$.

6 Calculation of the Associated Legendre Functions

Our goal now is to find out the value for $P_\nu^{-\mu}(x)$, where $|x| < 1$, $\mu \geqslant 0$ and $\nu \geqslant 0$. However, as this is a 'special' function, there are no explicit and elementary forms to evaluate these functions, so we will have to use approximation to the values. Though [17] only deals with the case when μ is a non-negative integer and $\nu \geqslant -\frac{1}{2}$ [17, 2.3], we will base our solution on their methods and take them to get function evaluations when μ and ν are *both* real numbers. Similar to what Olver and Smith have done in their paper, first we need to give a good approximation when the parameters μ and ν are relatively small: for example, when $\mu \in [0, 2)$ and $\nu \in [0, 2)$.

Instead of performing a series expansion as seen in [17, 4.1], this could be done with a spectral quadrature of the Schlaefli integral [15, p.174] [2]. Unfortunately, when the parameter μ is getting larger, this method will take longer computing time and refuse to reach convergence. In Fig. 15, we can see how the computing time change with μ:

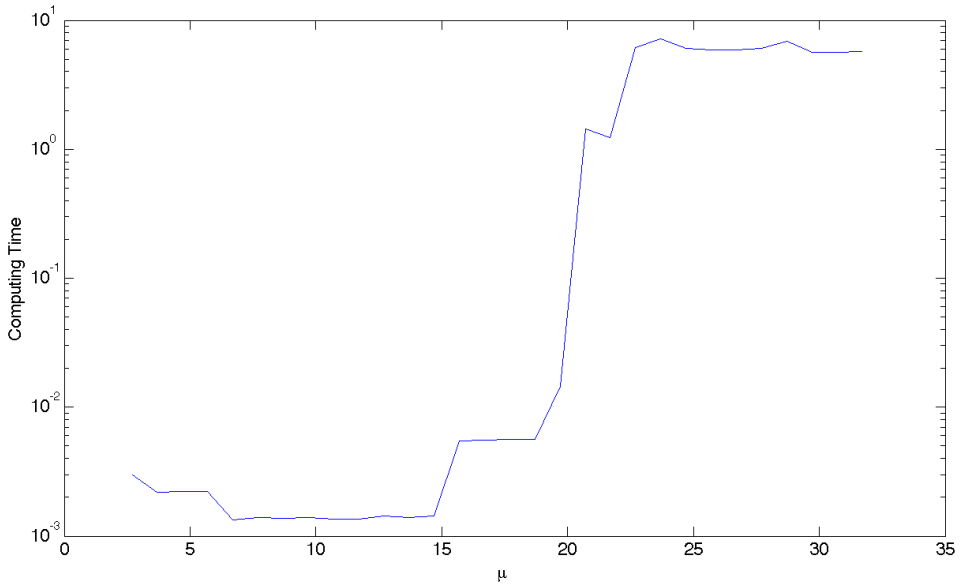

Figure 14: Computing time of $P_\nu^{-\mu}(0.35)$ with $\nu = 3.1$ and increasing μ

In order to obtain the values for the associated Legendre functions on

the full domain, we have to further apply recurrence relations between the functions with varying orders and degrees.

Olver and Smith's paper has provided us with two recursion formulas:

ν-wise Recursion Formula [17, 3.1]:

$$(\nu+\mu+1)\cdot P_{\nu+1}^{-\mu}(x)-(2\nu+1)x\cdot P_{\nu}^{-\mu}(x)+(\nu-\mu)\cdot P_{\nu-1}^{-\mu}(x)=0 \quad (52)$$

μ-wise Recursion Formula [17, 3.3]:

$$(\nu-\mu)(\nu+\mu+1)\cdot P_{\nu}^{-(\mu+1)}(x)-2\mu x(1-x^2)^{-\frac{1}{2}}\cdot P_{\nu}^{-\mu}(x)+P_{\nu}^{-(\mu-1)}(x)=0 \quad (53)$$

According to [17], when $x \geq 0$, recurring $P_{\nu}^{-\mu}(x)$ by the increasing ν direction or the decreasing μ direction is both stable. The latter means, we could start with an arbitrary initial condition at high enough μ and recur down suggested by Miller's method in [18, ch.6].

Hence, our strategy will be illustrated in the following step:

(1) Using the ν-wise recursion formula (52), we can get the value for $P_{\nu}^{-\mu}(x)$, where $\mu \in [0,1)$ and $\nu \geqslant 2$ as we know how to get the initial values $P_{\nu_s}^{-\mu}(x)$ and $P_{\nu_s+1}^{-\mu}(x)$, here ν_s stands for the fractional part of ν, or $\{\nu\} = \nu - \lfloor\nu\rfloor$ (Fig. 15).

(2) Next we calculate $P_{\nu}^{-\mu}(x)$ in the case when $\mu \geqslant 1$ and $\nu \geqslant 0$:

Let $\mu_s = \mu - \lfloor\mu\rfloor \in [0,1)$, we already know from (1) how to calculate $P_{\nu}^{-\mu_s}(x) =: P_1$. Now, we start at order μ_H and arbitrary initial values $P_{\nu}^{-\mu_H}(x) = 0$, $P_{\nu}^{-(\mu_H-1)}(x) = 1$ and then recur downward using the μ-wise Recursion Formula (53).

During the process, we record values of $P_{\nu}^{-\mu}(x) =: P_0$ and $P_{\nu}^{-\mu_s}(x) =: P_2$. Because P_2 is a scaled version of P_1 (we start the recursion with arbitrary initial values), the correct value for $P_{\nu}^{-\mu}(x)$ should be given by P_0P_1/P_2. This is illustrated in Fig. 16.

We validated the above method against Maple's evaluation of $P_{\nu}^{-\mu}(x)$, which applies for all real valued x, μ and ν. However, we found that this downwards μ-wise recurrence does not appear to couple into the correct solution $P_{\nu}^{-\mu}(x)$ when x is less than 0 or positive but close to 0, even though this recurrence direction should be stable (for $x > 0.2$, say, it works to machine precision). This is because if we place $x = 0$ into the equation (52), the recurrence is no longer a second-order difference equation. In consequence, Miller's algorithm will not work since recurrence is merely neutrally stable in either direction: i.e. we cannot begin at arbitrary initial values and recur downwards expecting that one solution will die out. For similar reasons, this

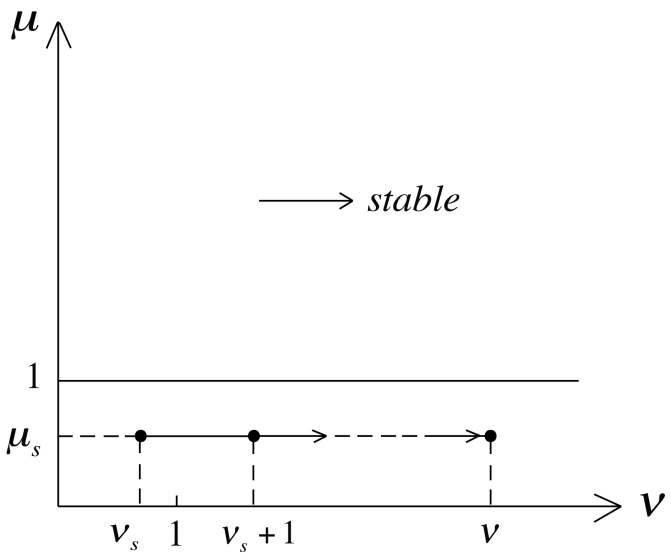

Figure 15: Use of ν-wise recurrence relation to evaluate associated Legendre function at arbitrary ν for small μ. Stable direction is shown.

problem also applies when x is near 0 [16]. Note that the result provided by Maple has a phase difference of $(-1)^{\mu/2}$ relative to the definitions used above [1, 17]. Table 2 shows the comparison of our result for $x = 0.69$ against phase-adjusted output from Maple. Our result matches Maple's result up to 15 digits.

From now on, we shall use Maple's solution since we find no other way to handle the case when x is negative or small and positive. However, we believe that our recurrence-based methods would ultimately be faster when chains of μ values at fixed (x, ν) are required.

Table 2: A Comparison of Results

	Recursion/Miller Alg.	Adjusted Maple Output
$P_{1.7}^{-1.3}(0.69)$	0.202044599910812	0.20204459991081169
$P_{17.1}^{-1.3}(0.69)$	0.002391703860784	0.00239170386078405
$P_{17.1}^{-15.8}(0.69)$	$0.5443728216591026 \times 10^{-20}$	$0.54437282165910212 \times 10^{-20}$

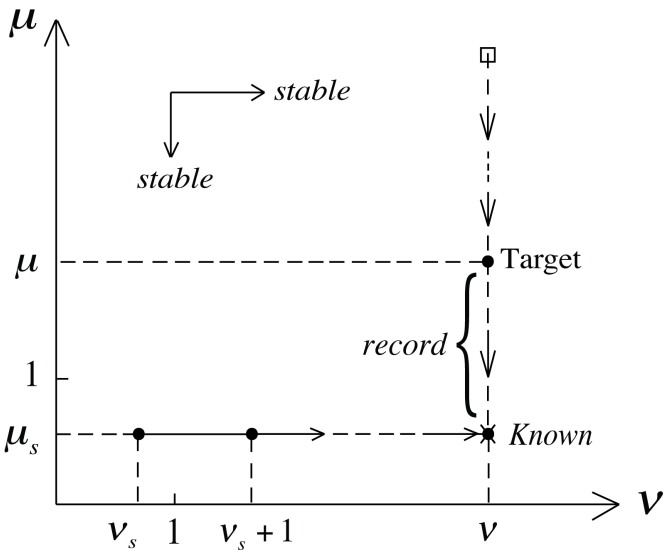

Figure 16: Use of ν-wise and μ-wise recurrence relations to evaluate associated Legendre function at arbitrary ν, μ. Stable directions are shown.

7 Geometry and Choice of Order for the Basis Function

When S^2 is viewed from directly above corner O, we have a picture that looks like Fig. 17. From the discussion of Sec. 5, each basis function will have the form:

$$u_{\mu,\nu}(\theta,\varphi) = P_\nu^{-\mu}(\cos\theta)\sin(\mu\varphi), \tag{54}$$

where ν is arbitrary and relates to the radial power.

Note that we are not interested in finding every eigenmode T_j of $D \subset S^2$. Instead, we will look for the ones with the high degree of symmetry that the BVP solution f must itself possess. To maintain the even symmetry about $\varphi = 3\pi/4$, we require that: $\sin(\frac{3\pi}{2}\mu) = 0$, which gives $\mu = \frac{2(2n-1)}{3} = \frac{4n-2}{3}$ for positive integer $n = 1, 2, 3, \cdots$.

Thus, the basis functions are:

$$U_n(\nu;\theta,\varphi) = P_\nu^{-\frac{4n-2}{3}}(\cos\theta)\cdot\sin(\frac{4n-2}{3}\varphi) \tag{55}$$

To visualize these basis functions, we can plot them on the sphere S^2, which is shown in Fig. 18.

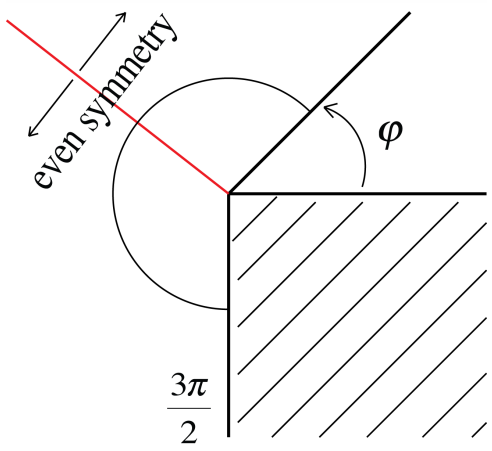

Figure 17: Top view on N pole of sphere

8 MPS on S^2 and Testing the Spherical Eigenmode Problem with Dirichlet BC

Due to the geometrical symmetry, we only need to focus on 1/6 of D, where D is 7/8 of the sphere S^2. Before we move on to matching the boundaries with Neumann BC, we first test the MPS by finding eigenmodes with Dirichlet BC on ∂D and Γ with odd symmetry about Γ and even symmetry about L on 1/3 of D, i.e. the shaded region in Fig. 19.

By picking the basis functions we select in the previous section, Dirichlet BC on 1/6 of the spherical triangle and the even symmetry is kept. Now, we have to choose a set of nodes along the geodesic Γ (BC=0 on Γ). We do so by finding a Gaussian quadrature for φ nodes in $[0, 3\pi/4]$ and calculating the corresponding θ values (see Appendix A). Then, for a fixed ν, we construct matrix A of size $N \times m$, where the n-th row of A represents the basis function $U_n(\nu)$ evaluated at each (θ, φ) nodes on the geodesic Γ (i.e. we select m nodes).

Next, we construct matrix B the same size of A, but with basis functions evaluated at random interior points in 1/6 of D. To get the random interior points so we still use the Gaussian quadrature for φ nodes in $[0, 3\pi/4]$, but for each of the φ node, we choose a random θ value that is inside the region. Thus, for a fixed ν, the n-th row of matrix B will be the basis function $U_n(\nu)$

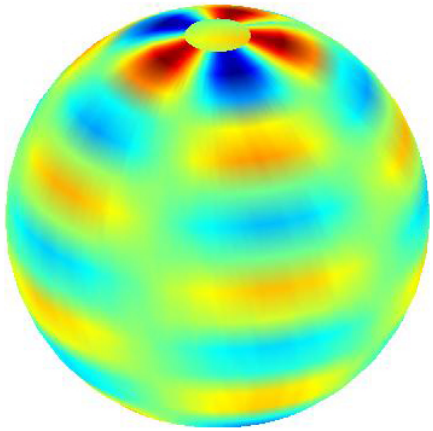

Figure 18: Color plot of basis function $u_{\mu,\nu}(\theta,\varphi)$ on S^2 for μ=2.53, ν=9.3

evaluated at these random (θ,φ) nodes.

For each ν, we can calculate the minimum generalized singular value $t(\nu) := \min_{u\in \text{ span }\{\xi_i\}} \frac{||u||_{L^2(\partial D)}}{||u||_{L^2(D)}}$ from the Generalized Singular Value Decomposition (GSVD) for matrix A and B [4] [2]. Fig. 20 shows $t(\nu)$ against ν for $\nu \in [1,10]$ when $N=15$, $m=20$.

The eigenvalues we are looking for are those ν values in Fig. 20 that locally minimizes $t(\nu)$. For example, the first five eigenvalues are approximately as follows: $\nu_1 = 1.71$, $\nu_2 = 2.99$, $\nu_3 = 4.27$, $\nu_4 = 4.55$, $\nu_5 = 5.49$.

To get more accuracy, we use Matlab's minimum locator $fminbnd$ which uses golden section search and parabolic interpolation [9]. Now we investigate if increasing N (number of basis functions with same ν) or m (number of nodes) will affect the accurate digits. Table 3 and Table 4 display the outputs for varying m and N.

Table 3: Eigenvalue ν_5 with $N=15$ and Increasing m

	$m=20$	$m=25$	$m=30$	$m=35$
ν_5	5.48791048513	5.48791054690	5.48791006353	5.48790995245
$t(\nu)$	0.00055712	0.000586185	0.000647697	0.000683122

As we can see from Table 3, changing the number of nodes does not give

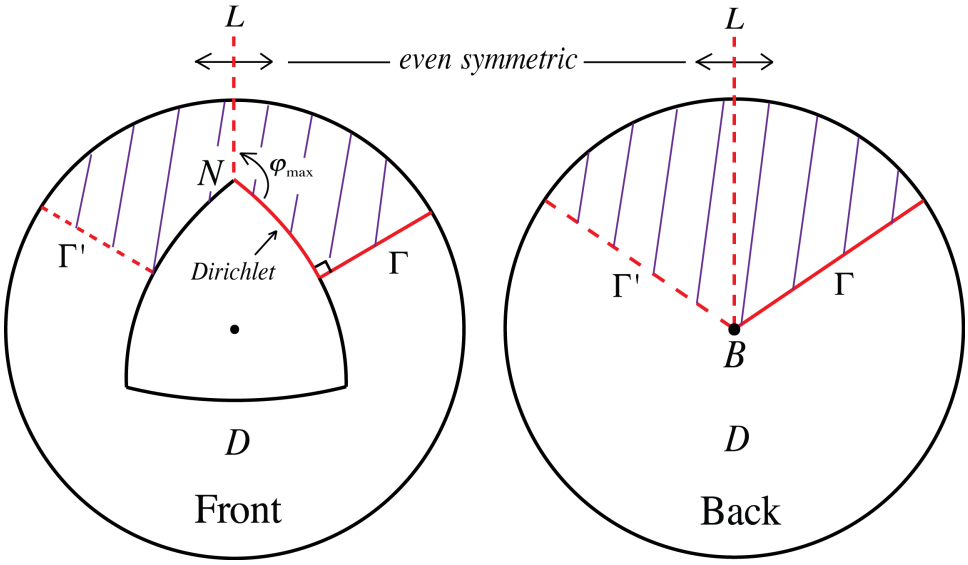

Figure 19: 1/6 of D with Dirichlet BC, front view and back view

Table 4: Eigenvalue ν_5 with $m = 50$ and Increasing N

	$N = 10$	$N = 20$	$N = 30$	$N = 40$
ν_5	5.48792245360	5.48791235986	5.48791211835	5.48791208662
$t(\nu)$	0.00217126	0.000350741	0.000117004	3.01014e-08

us more accurate digits for ν_5. However, as we can see from Table 4, the value of ν_5 slowly converges to 5 digits of accuracy (i.e. $\nu_5 = 5.48791$) when N increases to 50. The slow convergence we observed here is mainly due to the singularity about point B in Fig. 19. Another reason could be noise, which we show by zooming the interval around ν_5 in Fig. 21.

To visualize the eigenfunction which is a linear combination of the basis functions with fixed eigenvalue ν_5, we can plot it on the sphere along with L and geodesic Γ as shown in Fig. 22, which clearly indicates that the eigenfunction satisfies the Dirichlet boundary and preserves even symmetry about L.

Similarly, we can calculate the first four eigenvalues to 5 digits accuracy (listed in Table 5). In Fig. 23 we visualize the eigenfunctions for these eigenvalues.

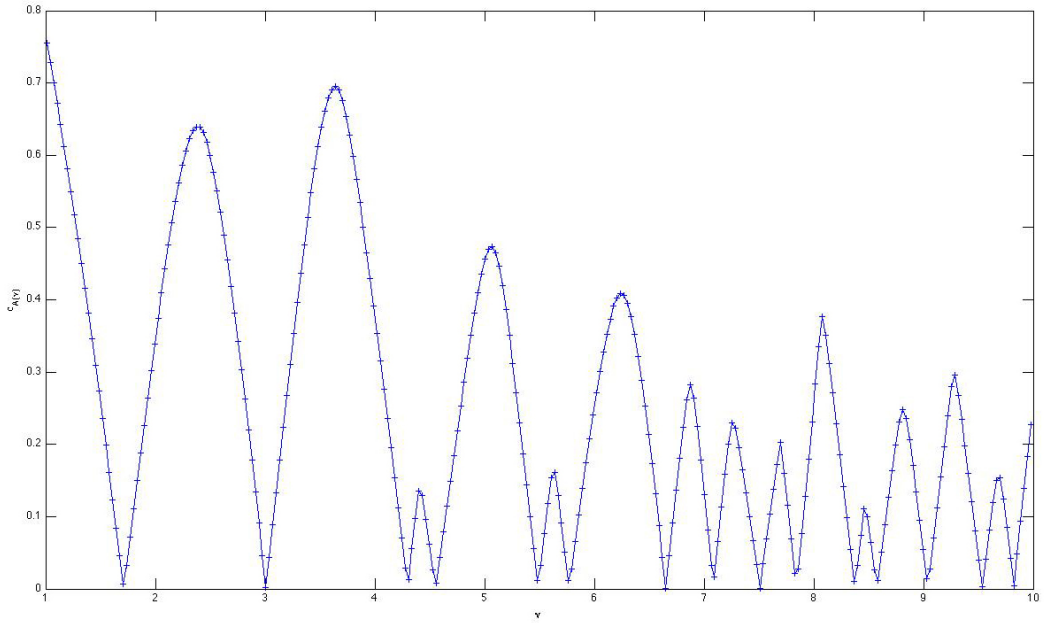

Figure 20: Min generalized singular value for A and B at different ν's

Table 5: First Five Eigenvalues to 5 Digits Accuracy

	ν_1	ν_2	ν_3	ν_4	ν_5
5 digits	1.71262	2.99330	4.27361	4.54764	5.48791

9 The Spherical Eigenmode Problem with Neumann BC

Recall that to solve the eigenvalue problem mentioned in Section 4 with MPS, we need our basis functions to be even symmetric about both L and Γ in Fig. 19. The even symmetry about Γ requires that $U_n = 0$ at node P on geodesic Γ, as shown in Fig. 24. As a result, we have an eigenvalue problem with Neumann boundary conditions. Appendix A gives the detail about how to choose the nodes along Γ and how to calculate the normal derivative of U at each of these nodes. Again, we construct matrix A of size $N \times m$, but now the n-th row of A represents the normal derivative of the basis function $U_n(\nu)$ evaluated at each (θ, φ) nodes on the geodesic Γ.

Similar to what we have done in the previous section, we perform GSVD

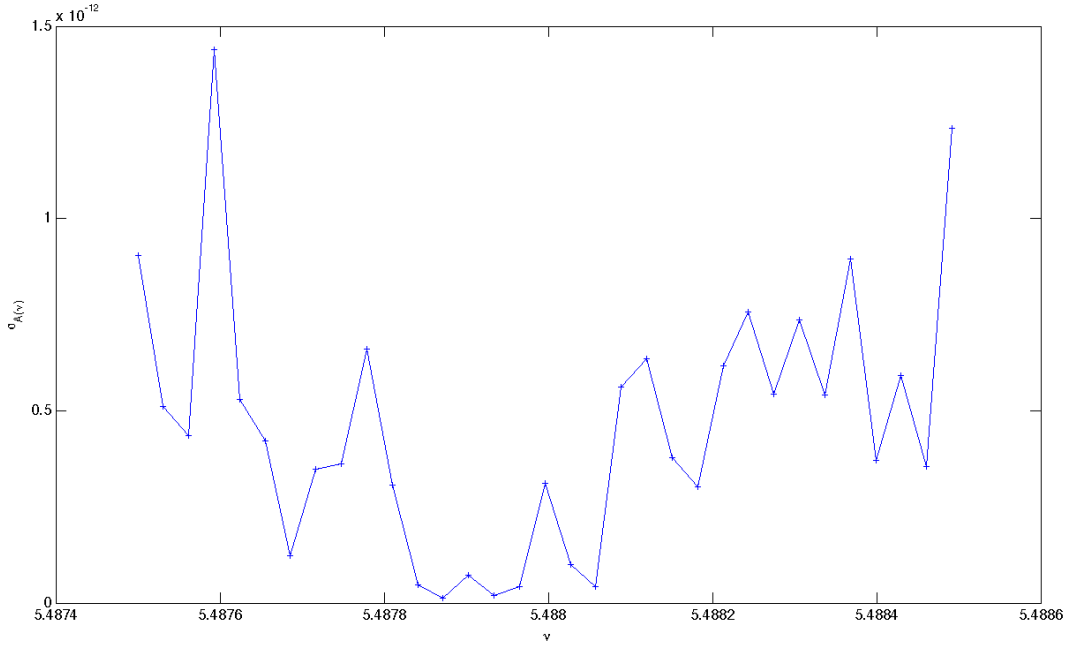

Figure 21: Value of $t(\nu)$ nearby ν_5 showing noise, $N = 15$, $m = 20$

on matrix A and B. However in Fig. 25, we find that $t(\nu)$ does not behave as what we have expected.

The failure of using GSVD here is due to the singularity at intersection B in Fig. 19. One way to handle this singularity is to put a cap at the back of sphere and solve for two separate set of basis functions (similar to what we have done in Section 2). Then, we will have to match the values and normal derivatives of these basis functions on the corresponding boundaries. We expect that this will fully solve the singularity as well as give us more accurate digits in the calculation of the eigenvalues.

10 Conclusion and Future Work

In this paper we have discussed the application of method of particular solutions (MPS) with domain decomposition technique to the BVP, which aims to deal with the corner singularity of the cube. We have demonstrated the method in calculating the capacity of the 2D unit square and have obtained the correct value of the capacity up to 15 digits of accuracy. We find that our

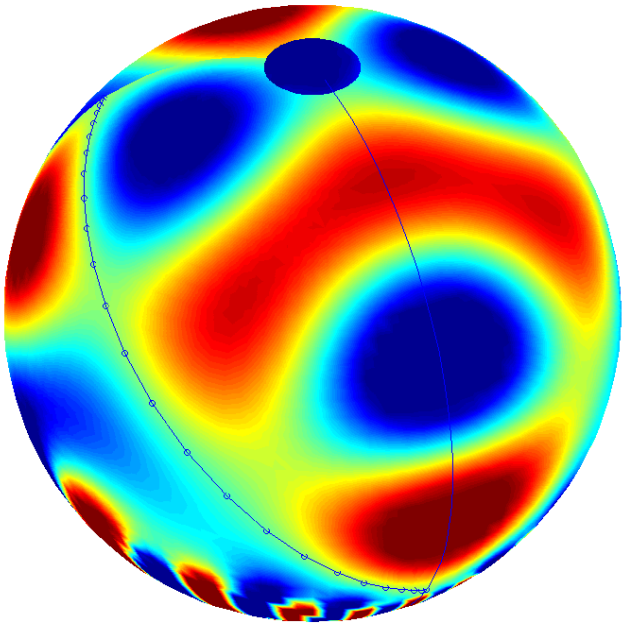

Figure 22: Eigenfunction on S^2 for ν_5=5.48791, $N = 25$, $m = 40$. Nodes along geodesic Γ is also shown.

result has an exponential error convergence rate of around 3 basis functions per accurate digit. For the 3D capacitance problem, we notice that solving the Laplace PDE involves solving a Dirichlet boundary eigenvalue problem on 7/8 of a sphere and finding the needed basis functions based at the corner of the cube. Fast algorithms for evaluating the required associated Legendre function are also discussed.

For the related Dirichlet eigenvalue problem, we got 5 digits accuracy for the eigenvalues on the sphere. In the future, we hope to solve the spherical eigenmode problem with Neumann boundary conditions with high accuracy. A possible approach to deal with the singularity at B in Fig. 19 is to place an imaginary cap at the back of the sphere and then separate and match the solutions as we did in the 2D capacity problem.

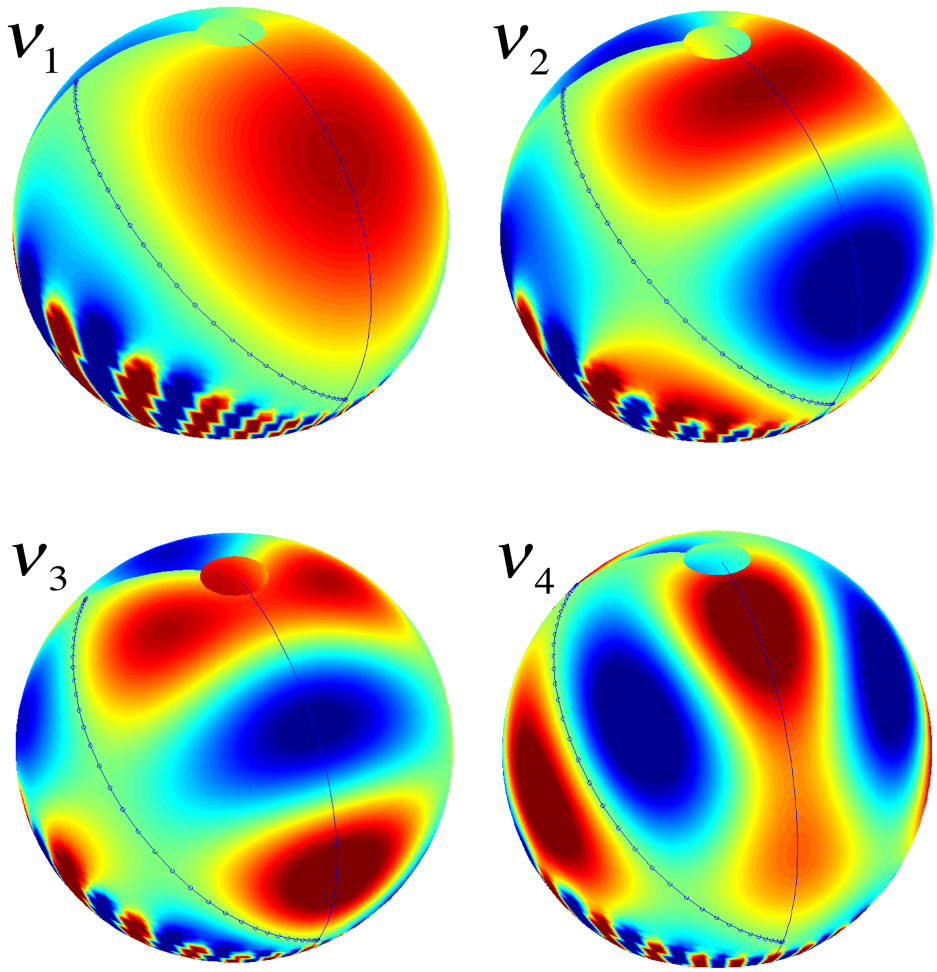

Figure 23: Dirichlet Eigenfunction on S^2, $N = 25$, $m = 40$

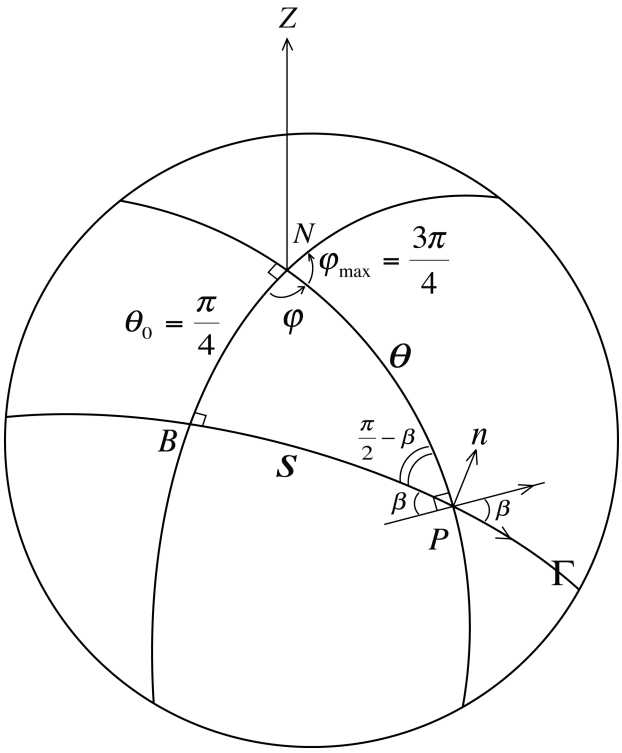

Figure 24: Matching boundary on the sphere

A Calculation of the Normal Derivatives

In this appendix we will explain how to compute normal derivatives of basis functions on the geodesic Γ.

(1) (θ, φ) coordinates of the surface normals

To pick points along the geodesic Γ more conveniently, we will choose a Gaussian quadrature on $[0, 3\pi/4]$ as the φ nodes, and we need to calculate the corresponding θ values (Fig. 26).

According to the spherical law of cosines,

$$\cos\theta = \cos\theta_0 \cdot \cos s + \sin\theta_0 \cdot \sin s \cdot \cos 90^\circ = \frac{\sqrt{2}}{2}\cos s \Rightarrow \cos s = \sqrt{2}\cos\theta. \quad (56)$$

On the other hand, according to the sine formula for spherical trigonometry,

$$\frac{\sin\theta}{\sin 90^\circ} = \frac{\sin s}{\sin\varphi} \Rightarrow \sin s = \sin\varphi \sin\theta. \quad (57)$$

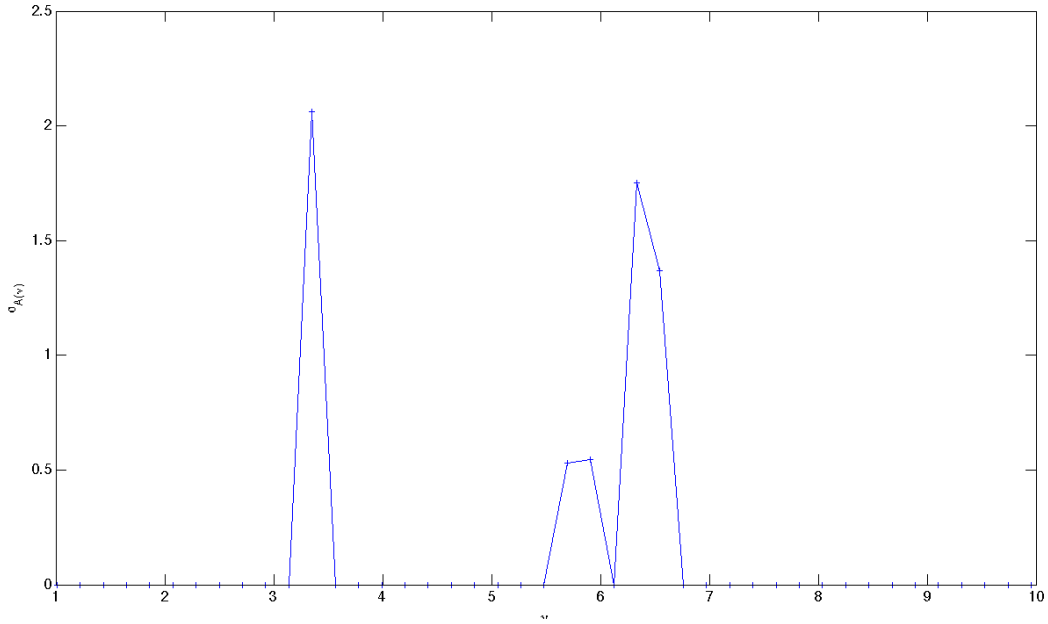

Figure 25: min generalized singular value for A and B at different ν's with Neumann BC

With (56) and (57), we have:

$$2\cos^2\theta + \sin^2\theta\sin^2\varphi = 1 \tag{58}$$

This yields:

$$\cos^2\theta = \frac{1-\sin^2\varphi}{1+\cos^2\varphi} \tag{59}$$

We notice that when $\varphi = \frac{\pi}{2}$, we also have $\theta = \frac{\pi}{2}$, as a result it is easy to see that $\cos\theta$ and $\cos\varphi$ will have the same sign. Taking the square root on both side of (59), we obtain:

$$\cos\theta = \frac{\cos\varphi}{\sqrt{1+\cos^2\varphi}}, \text{ or } \theta = \cos^{-1}\left(\frac{\cos\varphi}{\sqrt{1+\cos^2\varphi}}\right) \tag{60}$$

(2) Derivative of the associated Legendre function

We also can deduct the derivative of the associated Legendre function by recursion once we know how to evaluate the associated Legendre functions at given points.

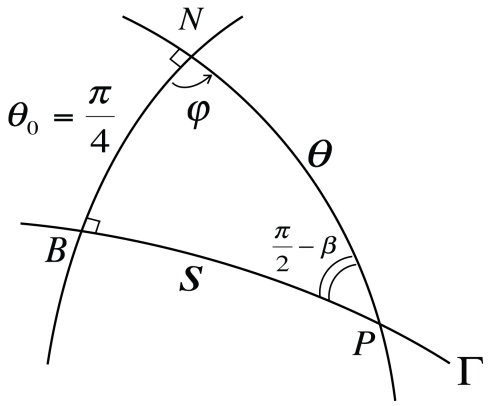

Figure 26: spherical triangle

The recursion is given by the following [1, 8.5.4]:

$$\frac{dP_\nu^{-\mu}(x)}{dx} = \frac{\nu x}{x^2-1} \cdot P_\nu^{-\mu}(x) - \frac{\nu-\mu}{x^2-1} \cdot P_{\nu-1}^{-\mu}(x), \text{ where } |x| < 1 \tag{61}$$

(3) Calculating the normals along the geodesic
By the definition of the normal derivative,

$$\frac{\partial u_i}{\partial n} = -\cos\beta \cdot \frac{\partial u_i}{\partial \theta} + \sin\beta \cdot \frac{\partial u_i}{\partial \varphi} \cdot \frac{1}{\sin\theta} \tag{62}$$

Here $u_i = P_\nu^{-\mu_i}(\cos\theta) \cdot \sin(\mu_i\varphi) = P_i(\cos\theta) \cdot \sin(\mu_i\varphi)$.
Replace $\cos\theta$ by x, from (61) we already know how to calculate $\frac{dP_i}{dx}$, so we can write

$$\frac{\partial u_i}{\partial n} = -\cos\beta \cdot \frac{dP_i}{dx} \cdot \frac{dx}{d\theta} \cdot \sin(\mu_i\varphi) + \sin\beta \cdot \frac{\partial u_i}{\partial \varphi} \cdot \frac{1}{\sin\theta}. \tag{63}$$

Therefore,

$$\frac{\partial u_i}{\partial n} = \cos\beta \cdot \sin\theta \cdot \frac{dP_i}{dx} \cdot \sin(\mu_i\varphi) + \frac{\sin\beta}{\sin\theta} \cdot P_\nu^{-\mu_i}(x) \cdot \mu_i \cdot \cos(\mu_i\varphi) \tag{64}$$

Finally, we need to calculate β in terms of θ. Again, by the sine formula for spherical trigonometry:

$$\frac{\sin\frac{\pi}{2}}{\sin\theta} = \frac{\sin(\frac{\pi}{2}-\beta)}{\sin\frac{\pi}{4}} = \sqrt{2}\cos\beta \tag{65}$$

This implies:

$$\cos\beta = \frac{\sqrt{2}}{2} \cdot \frac{1}{\sin\theta}, \text{ or } \beta = \cos^1(\frac{\sqrt{2}}{2} \cdot \frac{1}{\sin\theta}) \tag{66}$$

References

[1] M. Abramowitz and I. A. Stegun. *Handbook of Mathematical Functions with Formulas, Graphs, and Mathematical Tables*. Dover, New York, 10th edition, 1964.

[2] A. H. Barnett. Matlab code, 2009.

[3] T. Betcke. A GSVD formulation of a domain decomposition method for planar eigenvalue problems. *IMA J. Numer. Anal.*, 27:451–478, 2007.

[4] T. Betcke. The generalized singular value decomposition and the Method of Particular Solutions. *SIAM J. Sci. Comp.*, 30:1278–1295, 2008.

[5] T. Betcke and L. N. Trefethen. Reviving the method of particular solutions. *SIAM Rev.*, 47(3):469–491, 2005.

[6] A. Colesanti and P. Cuoghi. The Brunn-Minkowski inequality for the n-dimensional logarithmic capacity of convex bodies. *Potential Analysis*, 22(3):1–5, 2005.

[7] D. L. Colton. *Partial Differential Equations: An Introduction*. Dover Publications, 2004.

[8] W. Dijkstra and M. Hochstenbach. Numerical approximation of the logarithmic capacity. *Appl. Numer. Math.*, 2008. submitted.

[9] G. E. Forsythe, M. A. Malcolm, and C. B. Moler. *Computer Methods for Mathematical Computations*. Prentice-Hall, 1977.

[10] T. Hianik and V. I. Passechnik. *Bilayer Lipid Membranes*. Kluwer Academic Publishers Group, 1995.

[11] C.-O. Hwang and M. Mascagni. Electrical capacitance of the unit cube. *J. Appl. Phys.*, 95(7):3798–3802, 2004.

[12] R. Kress. *Linear Integral Equations*. Springer, New York, 2nd edition, 1999.

[13] G. Margaret and G. Shobha. A methodology for estimating interconnect capacitance for signal propagation delay in vlsls. *Microelectronics Journal*, 26(4):327–336, 1995.

[14] M. Mascagni and N. A. Simonov. The random walk on the boundary method for calculating capacitance. *J. Comput. Phys.*, 195(2):465–473, 2004.

[15] F. W. J. Olver. *Asymptotics and special functions*. Academic Press, New York, 1974.

[16] F. W. J. Olver. personal communication, 2009.

[17] F. W. J. Olver and J. M. Smith. Associated legendre functions on the cut. *J. Comput. Phys.*, 51(3):502–518, 1983.

[18] W. H. Press, S. A. Teukolsky, W. T. Vetterling, and B. P. Flannery. *Numerical recipes in C*. Cambridge University Press, Cambridge, 2nd edition, 2002.

[19] F. H. Read. Improved extrapolation technique in the boundary element method to find the capacitances of the unit square and cube. *J. Comput. Phys.*, 133(1):1–5, 1997.

[20] J. C. Strikwerda. *Finite difference schemes and partial differential equations*. Wadsworth Publ. Co., Belmont, CA, USA, 1989.